Available online at www.sciencedirect.com
SCIENCE DIRECT
International Journal of Heat and Mass Transfer 49 (2006) 1395–1402
International Journal of HEAT and MASS TRANSFER
www.elsevier.com/locate/ijhmt

Combined effects of inertia and thermophoresis on particle deposition onto a wafer with wavy surface

Chi-Chang Wang *

Department of Information Management, Hsing Kuo University of Management, No. 89, Yuying St., Tainan, Taiwan 709, ROC

Received 1 June 2005; received in revised form 27 September 2005
Available online 15 December 2005

Abstract

The effects of inertia, diffusion and thermophoresis on aerosol particle deposition from a stagnation point flow onto an axisymmetric wavy wafer are examined by the coordinate transformation and the cubic spline approximation. The numerical result reveals that the deposition effect is greatly controlled by the geometric shapes of the deposition surface and has a frequency similar to that of surface geometry. When diffusion and thermophoretic effects are the dominant deposition mechanism, the deposition effect affected by the displacement of the concaves and convexes on the deposition surface becomes obvious with the increase of radius, while the general mean deposition effect remains slightly less than that of flat wafer.

Keywords: Thermophoresis; Axisymmetric flow; Wavy surface; Cubic spline

1. Introduction

While a flow containing aerosol particles is passing through the surface of an object, the particles carried by the flow will cling to the surface under the interaction of Brown diffusion, gravity deposition, inertia effects as well as outside forces (for example: thermophoretic effect and electromagnetic effect). Relevant researches are playing an increasingly important role in engineering application and quality control of clean rooms. Review of past researches suggests that when the particles are very small, their adhesive rate is governed by diffusion and thermophoretic phenomena (for relevant researches, please refer to [1–4]). The so-called thermophoresis phenomenon refers to the behavior that particles float to colder area of the flow field under the push of heat arising from temperature gradient of the flow field. If analyzed by order of magnitude, this phenomenon can be obviously seen among particles of 0.1–1 μm in diameter. With the increase of diameter, the inertia of the particles is growing, making the particles more easily to stray the flowing route of the flow, thus the inertia effect gradually replaces diffusion and thermophoretic effects to become the dominant deposition mechanism. For relevant researches, please refer to [5–7].

As far as I know, no research about particle deposition effect of an irregular deposition surface was conducted. Whereas, in the actual industrial application, numerous tiny irregular surfaces are inevitably created during the manufacture and mechanic components or electronic circuits are often deliberately installed on the deposition surface. Therefore, it is necessary to further study the physical deposition phenomenon of an irregular surface. This essay focuses on the research of axisymmetric stagnant flow on deposition surface of a tinily wavy wafer under the interaction of coupling diffusion, thermophoretic and inertia effects, clarifies the displacement of the concaves and convexes on the deposition surface will forcibly change the moving direction of the flow, affect diffusion and inertia effects and influence the temperature gradient thus change particle thermophoretic phenomenon. The analytical method adopts the concept of Wang and Chen [8], starting

* Tel.: +886 6 2871928; fax: +886 6 2352973.
E-mail address: ccwang123@mail.hku.edu.tw

0017-9310/$ - see front matter © 2005 Elsevier Ltd. All rights reserved.
doi:10.1016/j.ijheatmasstransfer.2005.09.036

Nomenclature

a	amplitude of the wavy surface
D	diffusion constant
d_p	particle diameter
f	dimensionless streamfunction
g	gravitational acceleration
L	wavelength
N	particle concentration
p	pressure
Pr	Prandtl number
Re	Reynolds number
S	surface geometry function
Sc	Schmidt number
T	temperature
u_∞	r component of the velocity of the inviscid flow, evaluated at the wavy surface
u, w	r and z velocity components, respectively
V_d	local particle deposition velocity
$V_{d,m}$	mean particle deposition velocity

Greek symbols

α	thermal diffusivity
θ	dimensionless temperature
v	kinematic viscosity
σ	notation
λ	stagnation-point flow strength
ρ	density
ξ, η	coordinate
ψ	streamfunction

Superscript

–	dimensional quantity

Subscripts

w	surface conditions
∞	conditions far away from the surface

with the full Navier–Stokes equations and the concentration equation of coupling diffusion, inertia and thermophoretic effects, converting the complex boundary surface into a plane coordinate system through a simple conversion of coordinate, and calculating boundary layer equation arising from semi-similarity conversion by cubic spline approximation. One thing that needs to be addressed is that the deduction in this article proceeds from stream function' s point of view, which not only simplifies the complicated mathematic deduction but also gets equations simpler Wang and Chen [8]'s. Apart from the research on the relations between deposition effect and plane geometry, the article in the end specially discusses whether the mean deposition effect of wavy wafer is greater than that of flat wafer.

2. Governing equation

As shown in Fig. 1, consider an incompressible Newtonian fluid of which the concentration of aerosol particles is N_∞, passing through an geometrically symmetric irregular wafer of constant temperature T_w at a uniform velocity w_∞ and assume (a) it is a two-dimensional, axisymmetric and steady flow, (b) viscosity dissipation and buoyancy effect are ignored, (c) the particle concentration is very low and that on wall surface is zero, (d) when particles contact the wall surface, they will be absorbed by it and none will be bounced back. Under the above assumption, the mass, momentum, energy and particle concentration equations become

$$\frac{\partial \overline{u}}{\partial \overline{r}} + \frac{\overline{u}}{\overline{r}} + \frac{\partial \overline{w}}{\partial \overline{z}} = 0 \tag{1}$$

$$\overline{u}\frac{\partial \overline{u}}{\partial \overline{r}} + \overline{w}\frac{\partial \overline{u}}{\partial \overline{z}} = \frac{-1}{\rho}\frac{\partial \overline{p}}{\partial \overline{r}} + v\left(\nabla^2 \overline{u} - \frac{\overline{u}}{\overline{r}^2}\right) \tag{2}$$

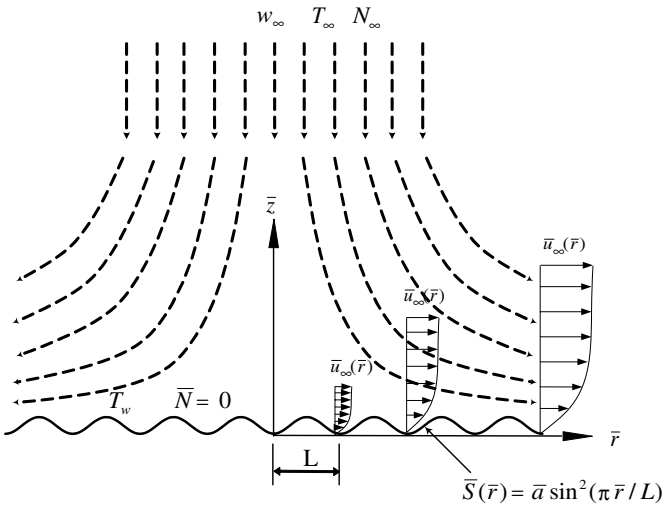

Fig. 1. Physical model and coordinates diagram.

$$\overline{u}\frac{\partial \overline{w}}{\partial \overline{r}} + \overline{w}\frac{\partial \overline{w}}{\partial \overline{z}} = \frac{-1}{\rho}\frac{\partial \overline{p}}{\partial \overline{z}} + v\nabla^2 \overline{w} \tag{3}$$

$$\overline{u}\frac{\partial T}{\partial \overline{r}} + \overline{w}\frac{\partial T}{\partial \overline{z}} = \alpha\nabla^2 T \tag{4}$$

$$\overline{u}\frac{\partial \overline{N}}{\partial \overline{r}} + \overline{w}\frac{\partial \overline{N}}{\partial \overline{z}} + \frac{\partial(\overline{u}_t\overline{N})}{\partial \overline{r}} + \frac{\partial((\overline{w}_t + \overline{w}_g)\overline{N})}{\partial z} = D\nabla^2 \overline{N} \tag{5}$$

where $\nabla^2 = \frac{\partial^2}{\partial \overline{r}^2} + \frac{1}{\overline{r}}\frac{\partial}{\partial \overline{r}} + \frac{\partial^2}{\partial \overline{z}^2}$. The boundary conditions at the surface $\overline{z} = \overline{S}(\overline{x})$ are

$$T = T_w, \quad \overline{u} = \overline{w} = \overline{N} = 0 \tag{6}$$

Whilst we have, on the upper surface

$$T = T_\infty, \quad \overline{N} = N_\infty, \quad \overline{u} = \overline{u}_\infty(\overline{r}), \quad \overline{p} = \overline{p}_\infty(\overline{r}) \tag{7}$$

where T and $\overline{N}$ are flow temperature and particle concentration, respectively; $\overline{u}$ and $\overline{w}$ are air flow velocities in the $\bar{r}$- and $\bar{z}$-direction, respectively. While, $\overline{u}_\infty$ can be considered as the velocity of inviscid fluid in $\bar{r}$ direction outside the boundary layer. $\overline{w}_g$ is the terminal sedimentation velocity that can be obtained by equating the Stokes drag to the gravitational force (Ye et al. [4] and Tsai and Liang [7])

$$\overline{w}_g = -\frac{\rho_p d_p^2 C}{18\mu_g} g \tag{8}$$

where μ_g is the air viscosity and C is the Stokes–Cunningham correction factor; $\overline{u}_t$ and $\overline{w}_t$ represent the particle thermophoretic velocities in directions along and perpendicular to radius that arise from temperature changes. Because the aerosol system is a system in which solid particles or liquid droplets form dispersed phase that floats in gaseous continuous phase. In an environment with unevenly distributed temperature, the aerosol particles will be driven by temperature gradient from a location with higher temperature to one with lower temperature. This kind of motion is called thermophoretic motion. According to the research by Talbot et al. [1], its mathematic expressions are as follows:

$$\overline{u}_t = -\frac{k_t v}{T}\frac{\partial T}{\partial \bar{r}} \tag{9}$$

$$\overline{w}_t = -\frac{k_t v}{T}\frac{\partial T}{\partial \bar{z}} \tag{10}$$

where $k_t v$ is thermophoretic diffusivity, whilst k_t is thermophoretic coefficient that can be expressed as

$$k_t = \frac{2C_s(\lambda_g/\lambda_p + C_t K_n)C}{(1+3C_m K_n)(1+2\lambda_g/\lambda_p + 2C_t K_n)} \tag{11}$$

where $K_n = \frac{2\lambda}{d_p}$ is Knudsen number that is the ratio of the mean free path of gas molecule to particle diameter, λ_g and λ_p represent the thermal conductivity coefficients of the gas and the aerosol particle respectively, Constant $C_s = 1.147$, $C_t = 2.20$ and $C_m = 1.146$ come from the results of the experiment (Shen [3]), C is an experimental constant that can be expressed as follows according to the suggestions put forward by Batchelor and Shen [2]

$$C = 1 + K_n(1.2 + 0.41e^{-0.88/K_n}) \tag{12}$$

In Eq. (11), although different particle has different size, its parameter k_t can range from 0.2 to 1.2, the k_t usually can be considered 0.5 when the particle diameter is less than 1.0 μm.

In order to make analysis possible, we first define velocity component and stream function $\overline{\psi}(\bar{r},\bar{z})$ as

$$\overline{u} = \frac{\partial\overline{\psi}}{\partial\bar{z}}, \quad \overline{w} = -\frac{\partial\overline{\psi}}{\partial\bar{r}} - \frac{\overline{\psi}}{\bar{r}} \tag{13}$$

to automatically meet mass conservation equation, thus no longer need Eq. (1). Secondly, out of analytical purpose, we define the following coordinate conversion:

$$\xi = \frac{\bar{r}}{L}, \quad \eta = (\bar{z} - \overline{S})\sqrt{\overline{u}_\infty/v\bar{r}} \tag{14}$$

and relevant dimensionless variables

$$\begin{aligned} f &= \frac{\overline{\psi}}{\sqrt{v\bar{r}\overline{u}_\infty}}, \quad \theta = \frac{T-T_\infty}{T_w - T_\infty}, \quad p = \frac{\overline{p}}{\rho U_0^2}, \\ u_\infty &= \frac{\overline{u}_\infty}{U_0}, \quad Re = \frac{U_0 L}{v}, \quad Pr = \frac{v}{\alpha}, \\ N &= \frac{\overline{N}}{N_\infty}, \quad w_g = \overline{w}_g/\sqrt{U_0 v/L}, \quad Sc = \frac{\mu}{\rho D}, \\ I &= -\frac{T_w - T_\infty}{T_\infty} = -\frac{\Delta T}{T_\infty} \end{aligned} \tag{15}$$

where I is the thermophoretic coefficient, $U_0 = \lambda L$ is the reference velocity, λ is the stagnation-point flow strength and can be estimated using the matching flow near the stagnation point with the viscous flow model. In the article, it can be approximated as (Cooper et. al [9])

$$\lambda = \frac{2w_\infty}{\pi R} \tag{16}$$

where R is the radius of the wafer.

The coordinate conversion in Eq. (14) adopts the theory of adjusting coordinate via the profile of irregular solid surface and converting irregular boundary into regular one. In addition, according to the traditional analysis on flow onto a wafer, the boundary thickness is proportionate to 1/2 power of the coordinate value in radial direction. For this reason, the whole coordinate system in Eq. (14) is stretched towards η direction. Noticeably, the above coordinate conversion is started with full Navier–Stokes equations and concentration equation, so, if the amplitude of the wavy surface stays at zero, the equation will resume to be the boundary layer equation for flat plate flow. In this way, by putting Eqs. (14) and (15) into Eqs. (2)–(5), we get

$$\begin{aligned} &\sigma f''' + \left(\frac{3}{2}f + \xi\left(\frac{f}{2}\frac{u'_\infty}{u_\infty} + f_\xi\right)\right)f'' - \xi\frac{p_\xi}{u_\infty^2} \\ &\quad + \left(S'\sqrt{Re\xi/u_\infty^2} + \frac{\eta}{2u_\infty^2}\left(1 - \xi\frac{u'_\infty}{u_\infty}\right)\right)p' \\ &\quad = \xi\left(f'_\xi f' + \frac{u'_\infty}{u_\infty}f'^2\right) + \frac{\Pi_1(f)}{Re^{1/2}} + \frac{\Pi_2(f)}{Re} \end{aligned} \tag{17}$$

$$\begin{aligned} &\sigma f''' + \left(\frac{3}{2}f + \xi\left(\frac{f}{2}\frac{u'_\infty}{u_\infty} + f_\xi\right)\right)f'' - S' - 1\sqrt{Re\xi/u_\infty^2}p' \\ &\quad = \xi\left(f'_\xi f' + \left(\frac{S''}{S'} + \frac{u'_\infty}{u_\infty}\right)f'^2\right) + \frac{\Pi_3(f)}{Re^{1/2}} + \frac{\Pi_4(f)}{Re} \end{aligned} \tag{18}$$

$$\begin{aligned} &\frac{\sigma}{Pr}\theta'' + \frac{1}{2}\left(3 + \xi\frac{u'_\infty}{u_\infty}\right)f\theta' \\ &\quad = \xi(f'\theta_\xi - f_\xi\theta') + \frac{\Pi_5(f)}{Re^{1/2}} + \frac{\Pi_6(f)}{Re} \end{aligned} \tag{19}$$

$$\begin{aligned} &\frac{\sigma}{Sc}N'' + \left(\frac{f}{2}\left(3 + \xi\frac{u'_\infty}{u_\infty}\right) - w_g\left(\frac{\xi}{u_\infty}\right)^{1/2}\right)N' \\ &\quad - \frac{Ik_t\sigma}{1-I\theta}\left(\frac{IN}{1-I\theta}\theta'^2 + N'\theta' + N\theta''\right) \\ &\quad = \xi(f'N_\xi - f_\xi N') + \frac{\Pi_7(f)}{Re^{1/2}} + \frac{\Pi_8(f)}{Re} \end{aligned} \tag{20}$$

where $'$ and ξ are partial derivatives $\frac{\partial}{\partial\eta}$ and $\frac{\partial}{\partial\xi}$, respectively; $\sigma = 1 + S'^2$, while the eight operators $\Pi_1 \sim \Pi_8$ are the set of terms with coefficient $Re^{-1/2}$ or Re^{-1}. As the terms are considerably complex and will be rounded down in the later deduction, they are not listed here.

From Eq. (17), we can see the pressure gradient p' in η direction is $O(Re^{-1/2})$, indicating the pressure gradient in ξ direction can be obtained from the inviscid fluid outside the boundary layer, as shown below

$$p_\xi = -\left(\sigma u_\infty u'_\infty + S'S'' u_\infty^2\right) \tag{21}$$

When Reynolds number is too big (i.e. the boundary layer theory is applicable), after removing p' from Eqs. (17) and (18) and rounding down $\Pi_1 \sim \Pi_8$, by order magnitude analysis, we obtain the following boundary layer equations:

$$\sigma f''' + \frac{1}{2}\left(3 + \xi\frac{u'_\infty}{u_\infty}\right) f f'' - \xi\left(\frac{S'S''}{\sigma} + \frac{u'_\infty}{u_\infty}\right)(f'^2 - 1) = \xi\left(f'_\xi f' - f_\xi f''\right) \tag{22}$$

$$\frac{\sigma}{Pr}\theta'' + \frac{1}{2}\left(3 + \xi\frac{u'_\infty}{u_\infty}\right) f\theta' = \xi(f'\theta_\xi - f_\xi\theta') \tag{23}$$

$$\frac{\sigma}{Sc}N'' + \left(\frac{f}{2}\left(3 + \xi\frac{u'_\infty}{u_\infty}\right) - w_g\left(\frac{\xi}{u_\infty}\right)^{1/2} - \frac{Ik_t\sigma}{1 - I\theta}\theta'\right)N' - \frac{Ik_t\sigma}{1 - I\theta}\left(\frac{I}{1 - I\theta}\theta'^2 + \theta''\right)N = \xi(f'N_\xi - f_\xi N') \tag{24}$$

together with the boundary conditions,

$$\theta = 1, \quad f = N = 0, \quad f' = 0 \quad \text{at } \eta = 0 \tag{25}$$

$$\theta = 0, \quad f' = N = 1 \quad \text{as } \eta \to \infty \tag{26}$$

To solve the preceding equations, we have to know the distribution of speed u_∞ outside the boundary layer in ξ direction. In this article, we compute the flow field outside the boundary layer through coordinate conversion and by SOR method, of which the stream function equation and coordinate conversion equation are

$$\frac{\partial^2\overline{\psi}}{\partial\overline{r}^2} + \frac{1}{\overline{r}}\frac{\partial\overline{\psi}}{\partial\overline{r}} - \frac{\overline{\psi}}{\overline{r}^2} + \frac{\partial^2\overline{\psi}}{\partial\overline{z}^2} = 0 \tag{27}$$

$$r = \overline{r}/L, \quad z = (\overline{z} - \overline{S})/L \tag{28}$$

put Eq. (28) into Eq. (27), we obtain the following stream function equation and the expression of u_∞:

$$\frac{\partial^2\psi}{\partial r^2} + \frac{1}{r}\frac{\partial\psi}{\partial r} - \left(\frac{S'}{r} + S''\right)\frac{\partial\psi}{\partial z} - 2S'\frac{\partial^2\psi}{\partial r\partial z} - \frac{\psi}{r^2} + \sigma\frac{\partial^2\psi}{\partial z^2} = 0 \tag{29}$$

$$u_\infty = \left.\frac{\partial\psi}{\partial z}\right|_{z=0} \tag{30}$$

The result is shown in Fig. 2, from which we can see the impact of wavy surface on flow field is: the speed of a flow is accelerated on an ascending wavy surface (from wave trough to wave crest with slope S' being positive) and decelerated on a descending wavy surface (from wave crest to wave trough with slope S' being negative). u_∞ has a same periodical distribution as wavy surface. One thing deserving attention is the variation amplitude of speed u_∞ is in direct proportion to the amplitude of surface waveform and becomes more obvious with the increase of radius.

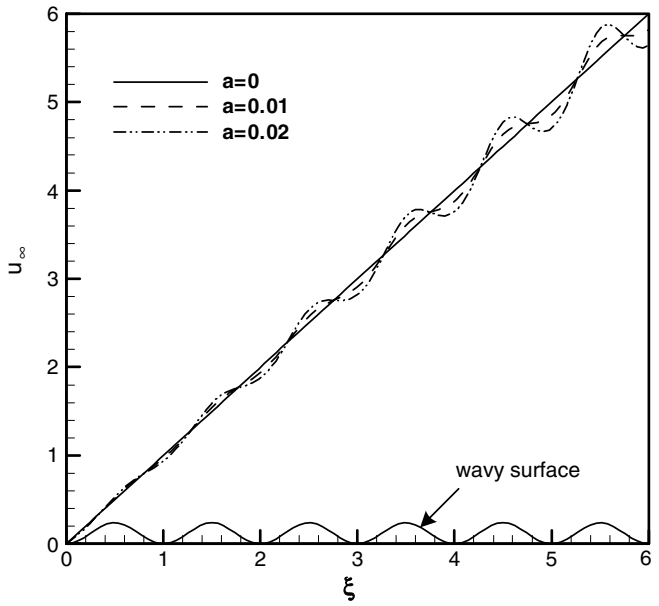

Fig. 2. Axial distribution of u_∞.

Since the governing equation for a flow has been established, in order to research into deposition effect, we define local deposition velocity, which due to varied along the wavy surface, of the system as

$$V_d = \frac{J}{N_\infty} \tag{31}$$

where J is particle flux per unit area of wavy surface, which general expression is

$$J(\overline{r}) = \left(-D\frac{\partial\overline{N}}{\partial n} + (\overline{V} + \overline{V}_t + \overline{V}_g)\overline{N}\right)_{\overline{z}=\overline{S}(\overline{r})} \tag{32}$$

where $\frac{\partial\overline{N}}{\partial n}$ is the concentration gradient on vertical wall, $\overline{V}$, $\overline{V}_t$ and $\overline{V}_g$ are flow velocity, thermophoretic velocity and terminal sedimentation velocity on vertical wall, respectively. Put Eq. (32) into Eq. (31), as the particle concentration on the wall is zero, we get the following simplified equation:

$$V_d = \frac{\sqrt{\nu\alpha\sigma u_\infty/\xi}}{Sc}N'|_{\eta=0} \tag{33}$$

Additionally, we define mean deposition velocity as

$$V_{d,m} = \frac{J_m(\overline{x})}{N_\infty} \tag{34}$$

where the mean particle flux J_m is the aggregate value of particle flux integrated along deposition surface and divided by the vertical projected area as shown in the following mathematical expression:

$$J_m(\overline{x}) = \frac{1}{\pi\overline{r}^2}\int_0^{\overline{r}} 2\pi\overline{r}\sqrt{\sigma}J\,d\overline{r} \tag{35}$$

Put Eq. (35) into Eq. (34), we get the following integral relation:

$$V_{\mathrm{d,m}} = \frac{2\sqrt{v\alpha}}{Sc\xi^2}\int_0^{\xi}\sigma\sqrt{\xi u_\infty}N'|_{\eta=0}\mathrm{d}\xi \tag{36}$$

3. Numerical method

According to the numerical method adopted in this article, all the differential terms in η direction are dealt by cubic spline approximation, while all the differential terms in ξ are discretized by four-point backward differenced method. As cubic spline approximation can discretize the governing equation into the algebraic expression only containing functions or the algebraic expression of the first or second derivative that are continuous in all computation areas, we firstly change Eqs. (22)–(24) into the following standard expression with the concept of virtual time (Wang and Kahawita [10]):

$$g_{i,j}^{n+1} - G_{i,j}g_{i,j}'^{n+1} - S_{i,j}g_{i,j}''^{n+1} = F_{i,j} \tag{37}$$

where function g represents f' or θ or N. In Eq. (37), the method of order reduction is used to first get the values $f_{i,j}'^{n+1}$, $f_{i,j}''^{n+1}$ and $f_{i,j}'''^{n+1}$ on grid points, after that, according to the theory of cubic spline, any function $g(y)$ at any point of sub-space ($y_j \leqslant y \leqslant y_{j+1}$) can be expressed with the functions and derivative values of two ends as

$$\begin{aligned} g(y) = {} & g_{j-1}''\frac{(y_j-y)^3}{6\Delta y_j} + g_j''\frac{(y-y_{j-1})^3}{6\Delta y_j} \\ & + \left(g_{j-1} - \frac{g_{j-1}''\Delta y_j^2}{6}\right)\frac{y_j-y}{\Delta y_j} \\ & + \left(g_j - \frac{g_j''\Delta y_j^2}{6}\right)\frac{y-y_{j-1}}{\Delta y_j} \end{aligned} \tag{38}$$

where $\Delta y_j = y_j - y_{j-1}$ is grid space. Therefore, in Eqs. (22)–(24), the functional value of grid point f can be accurately solved with the following equation:

$$\begin{aligned} f_{i,j} &= \int_0^{y_j} f'\mathrm{d}\eta \\ &= \sum_{k=1}^{j}\left(\left(f_{i,k-1}' + f_{i,k}'\right)\frac{\Delta y_k}{2} - \frac{\Delta y_k^3}{24}\left(f_{i,k-1}''' + f_{i,k}'''\right)\right) \end{aligned} \tag{39}$$

In Eqs. (33) and (34), the values of coefficients, such as $F_{i,j}$, $G_{i,j}$ and $S_{i,j}$, can be determined by the solutions obtained in previous time. In addition, as the value of Schmidt number for aerosol particle is much bigger than the value of Prandtl number, taking the particle of 0.01 μm–10 μm in diameter for example: the value of Schmidt number may ranges from 300 to 10^5, the particle concentration boundary layer is much smaller than velocity and temperature boundary layers. What is more, when the temperature of wall surface is as low as that of cold wall surface ($\Delta T < 0$), the thermophoretic effect will change sharply in concentration very near the wall, though the effect of thermophoresis was significant throughout the thermal boundary layer. Therefore, the collocation of grid points for concentration equation is different from those for velocity and temperature equations. The former has to set more points in area very near wall surface where the temperature, temperature gradient and velocity can be computed with Eq. (38), thus avoiding error caused by traditional difference method.

4. Results and discussion

In order to know the character of particle deposition to irregular surface, the article uses regular wavy curved surface to study the impact of concave and convex geometrical shapes of deposition surface on particle deposition. The dimensionless form of plane geometry is $S(x) = a\sin^2(\pi x)$, where a is wavy amplitude–wavelength ratio. As for environment parameter, polystyrene latex (PSL) aerosol flow experiment (Ye et al. [4]) in a typical clean room is referred, in the experiment, it is considered that gas which temperature is 300 K, Prandtl number is 0.72 and carries particles of $\rho_{\mathrm{p}} = 1027\ \mathrm{kg\,m^{-3}}$ passes through a wafer of 10 cm in diameter at a speed $w_\infty = 30\ \mathrm{cm\,s^{-1}}$. In the article, Eq. (16) is used to calculate the corresponding flow strength $\lambda = 3.82\ \mathrm{s^{-1}}$. The comparison between this result and that obtained from Ye et al. [4] is shown in Fig. 3, from which we can see the data obtained in this article tally with the experimental data.

Fig. 4 is the distribution of local deposition velocity along wavy surface under different wavy amplitude–wavelength ratio. Figs. 5 and 6 are the distribution schematic diagrams of flow velocity field, temperature field and particle concentration field when the wavy amplitude–wavelength ratio is 0.02. From Fig. 4, we can see that on

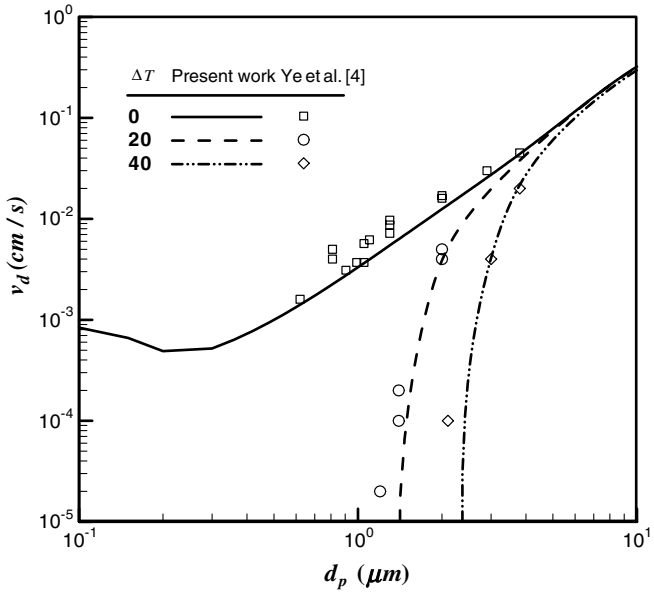

Fig. 3. A comparison of deposition velocity for flat wafer between numerical results from present work and experimental data from Ye et al. [4] with different temperature.

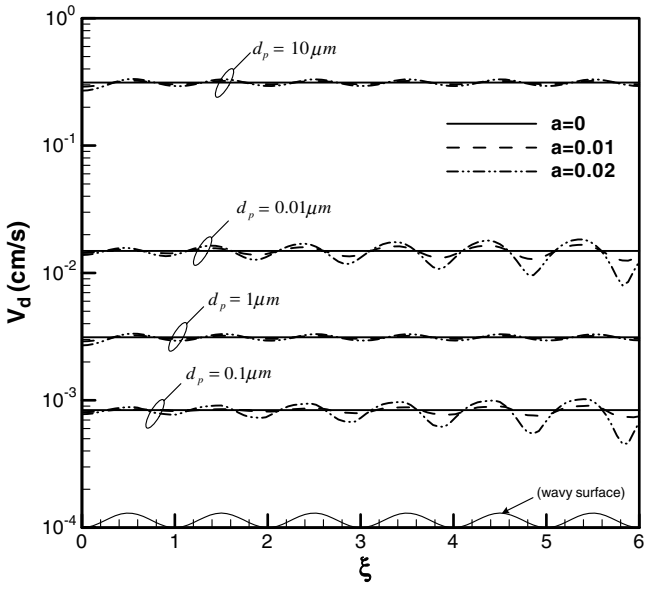

Fig. 4. Distribution of the local deposition velocity for various values of d_p and wavy amplitude–wavelength ratio at $\Delta T = 0$.

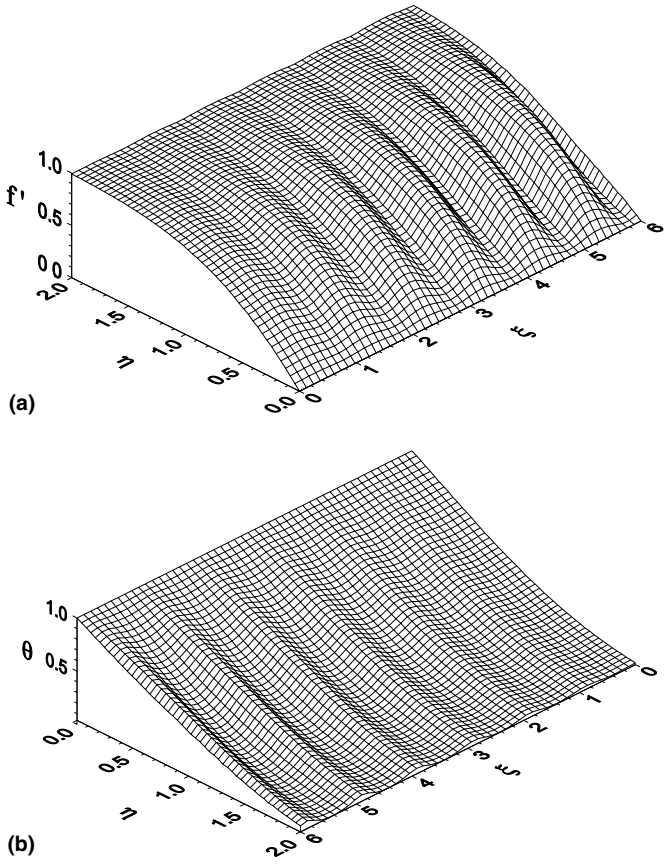

Fig. 5. Distribution of velocity of dimensionless flow field f' and temperature θ when wavy amplitude–wavelength ratio is 0.02: (a) distribution of velocity field and (b) distribution of temperature field.

a flat plate (i.e. $a = 0$), the local deposition velocity for particles of various diameters is a constant, while on a wavy

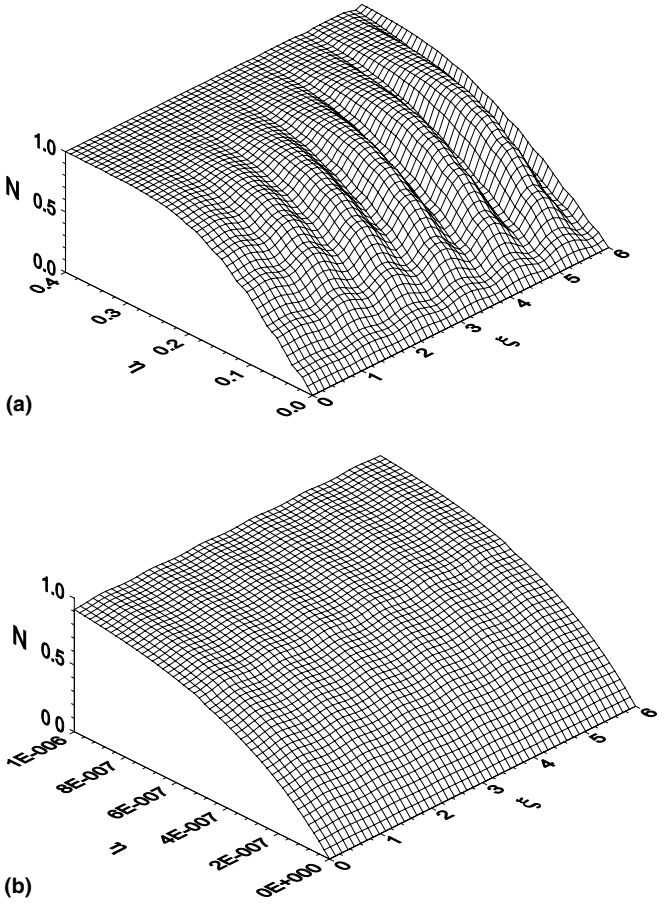

Fig. 6. Distribution of dimensionless particle concentration when wavy amplitude–wavelength ratio is 0.02 and $\Delta T = 0$: (a) $d_p = 0.01$ μm and (b) $d_p = 10$ μm.

plate, it shows as expected the frequency of variation is almost same as that of deposition surface geometry, its variation amplitude increases with the increase of the wavy amplitude–wavelength ratio. Notably, in Figs. 4 and 6a, we found when particle diameter is 0.01 or 0.1 μm, their variation amplitude increases with the increase of radius, that is obviously different from the result for the particles which diameter is between 1 μm and 10 μm. It can be explained as when particle diameter is small, the particle inertia is small, and convection and diffusion are the dominant deposition mechanism, therefore, in Figs. 6a and 5a, the distribution of particle concentration and flow velocity shows an increasing trend of variation amplitude with the increase of radius, that is the result of affected diffusion effect by the flow field. On the other hand, when the particle diameter is more than 1 μm, inertia effect obviously replaces diffusion effect and the deposition is no longer affected by flow velocity, therefore, in Fig. 6b, the variation amplitude of particle concentration does not increase with the increase of radius.

Fig. 7 compares the distributions of local deposition velocity of wavy plate and flat plate against radius under various temperature difference between wall surface and ambient when the particle diameter $d_p = 0.1$ μm, from

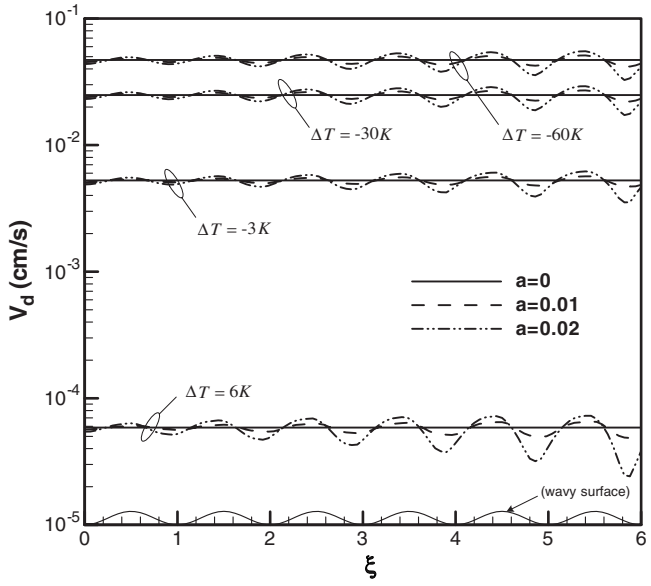

Fig. 7. Distribution of the local deposition velocity for various values of ΔT and wavy amplitude–wavelength ratio at $d_p = 0.1$ μm.

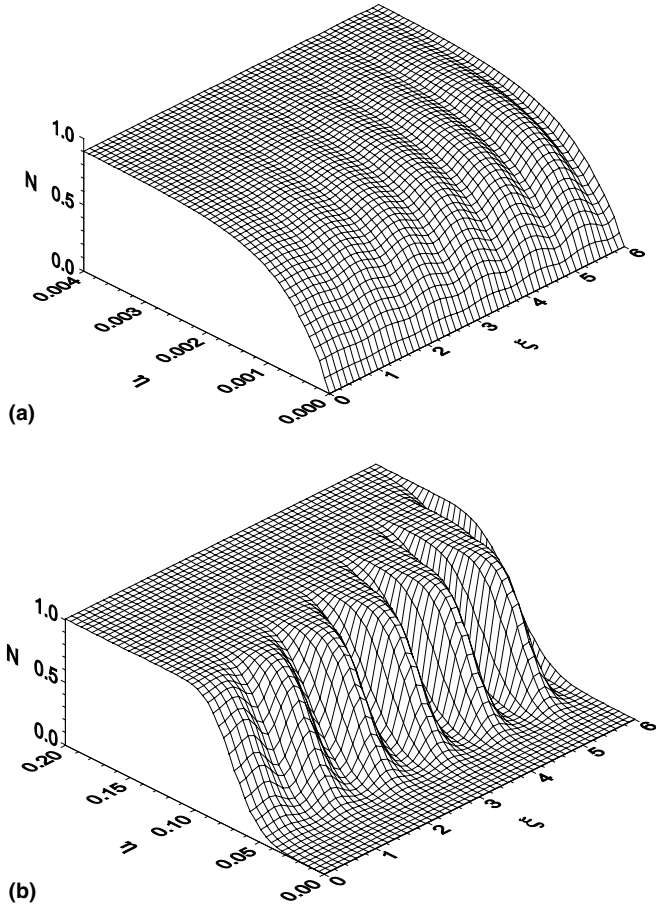

Fig. 8. Distribution of dimensionless particle concentration when wavy amplitude–wavelength ratio is 0.02 and $d_p = 0.1$ μm: (a) $\Delta T = -60$ K and (b) $\Delta T = 6$ K.

which we can see when the wall surface is colder than ambient (i.e. $\Delta T < 0$), the local deposition velocity increases, resulting from the accelerated deposition of aerosol particles onto the wall surface under the influence of thermophoresis. If consulting Fig. 8a in the meantime, we can more clearly see that the universal existence of thermophoresis in the heat boundary layer not only causes the dimensionless particle concentration near concentration boundary layer slightly less than 1, but also leads to a sharp change of particle concentration in area very near the wall surface as a result of thinner concentration boundary layer. Contrarily, when the wall surface is hotter than the ambient (i.e. $\Delta T > 0$), the aerosol particles will be driven away from the wall surface, resulting in decreased local deposition velocity. Moreover, when the effect of thermophoresis featuring hot wall surface expelling particles away from it is bigger than the effects of Brown diffusion and inertia, it may even result in an area near the plate surface which particle concentration is approximately zero as shown in Fig. 8b. Besides, in Fig. 7, no matter whether the deposition surface is cold or hot wall surface, the local deposition velocity of wavy surface presents a periodical change same as that of wavy surface, and its variation amplitude considerably increases with the increase of radius, it can be explained as the effects of diffusion and thermophoresis outshine inertia effect and the deposition effect is deeply affected by flow field and temperature field. Therefore, the concentration distribution shown in Fig. 8 is same as the distribution of velocity field and temperature field shown in Fig. 5, i.e. their variation amplitudes all become increasingly obvious with the increase of radius.

In order to research into the impact of wavy plate on the total deposition velocity, Figs. 9 and 10 show the distribution of mean local deposition velocity along wavy surface.

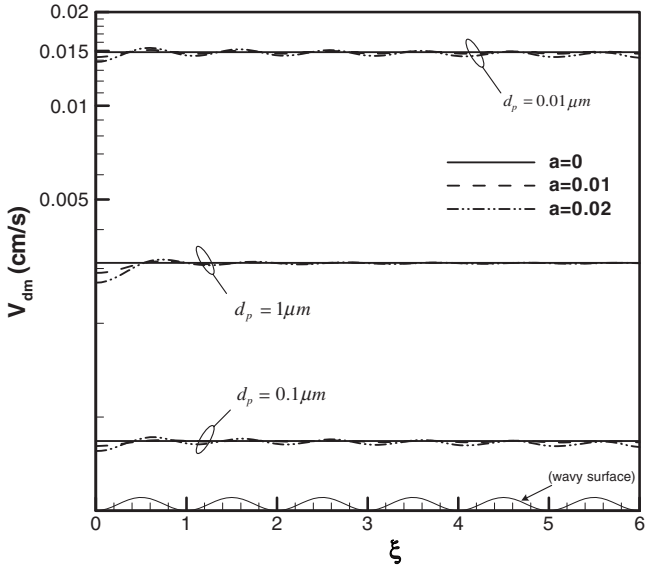

Fig. 9. Distribution of the mean deposition velocity for various values of wavy amplitude–wavelength ratio and $\Delta T = 0$.

As mean deposition velocity is the average value of the local deposition velocity integrated along wavy surface, it

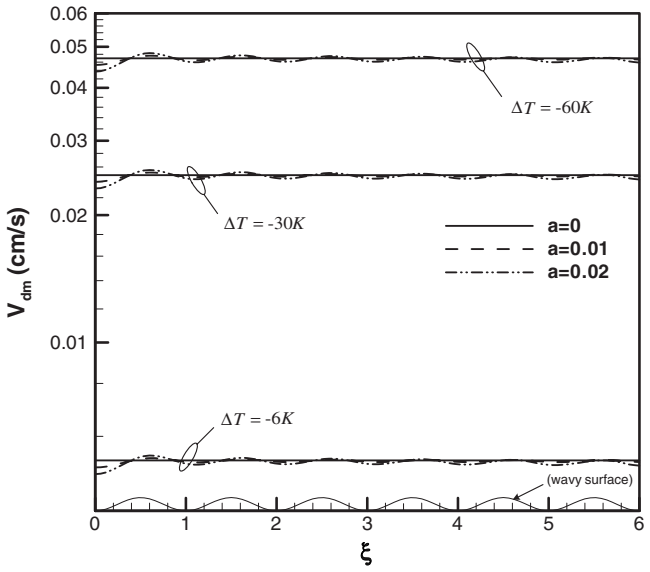

Fig. 10. Distribution of the mean deposition velocity for various values of ΔT and wavy amplitude–wavelength ratio at $d_p = 0.01$ μm.

can be seen that under the integral effect, the variation of mean deposition velocity in the center of the plate is most remarkable. Noticeably, in Figs. 9 and 10, only when the particle diameter is 1 μm and the temperature of the wall surface is equal to that of ambient ($\Delta T = 0$), the variation of mean deposition velocity becomes less remarkable against the radius increase. In other cases, it maintains basically unchanged amplitude as the radius increases. When inertia is the dominant deposition mechanism (for instance: when $d_p = 1$ μm and $\Delta T = 0$), with the increase of radius, the mean deposition velocity is approximate to that of flat surface. On the other hand, when diffusion and thermophoretic effects outshine inertia effect, it becomes slightly less than that of flat plate and shows approximately same variation amplitude.

5. Conclusions

This article discussed from an approach of mathematic theory how the tiny extruded and depressed displacement on a wafer affect deposition effect. Through comparison, it is found that numerical result surprisingly tallies with the experimental result for flat wafer, indicating this article result can be effectively applied to the analysis of emulated flat plate and surface with tiny undulations. From the numerical result, we can see that the local deposition velocity is obviously controlled by surface geometry, showing same distribution of frequency as that of surface geometry. Its amplitude is in direct proportion to the amplitude of wavy surface, and when inertia effect is less than diffusion and thermophoretic effects, its amplitude increases with the increase of radius. From a general point of view, the mean deposition effect of wavy plate is slightly less than that of flat wafer, showing that although, with a same projected area, the deposition area of wavy surface is more than the deposition area of flat plate and the extruded area on wavy surface helps increase deposition effect, the deposition effect of wavy surface near depressed area is less than that of flat plate. That means the tiny electronic components or displacement on deposition surface can be ignored in engineering application if only the total deposition effect is mattered.

Acknowledgement

Thanks for the subsidy of the Outlay 93-2212-E-432-001 given by National Science Council, the Republic of China, to help us finish this special research successfully.

References

[1] L. Talbot, R.K. Cheng, R.W. Scheffer, D.P. Wills, Thermophoresis of particle in a heated boundary layer, J. Fluid Mech. 101 (4) (1980) 737–758.
[2] G.K. Batchelor, C. Shen, Thermophoretic deposition in gas flow over cold surface, J. Colloid Interface Sci. 107 (1) (1985) 21–37.
[3] C. Shen, Thermophoretic deposition of particles onto cold surface of bodies in two dimensional and axi-symmetric flows, J. Colloid Interface Sci. 127 (4) (1989) 104–115.
[4] Y. Ye, D.Y.H. Pui, B.Y.H. Liu, S. Opiolka, S. Blumhorst, H. Fissan, Thermophoretic effect of particle deposition on a free standing semiconductor wafer in a clean room, J. Aerosol Sci. 22 (1) (1991) 63–72.
[5] F. Belosi, V. Prodi, Particle deposition within the inertial spectrometer, J. Aerosol Sci. 18 (1) (1987) 37–42.
[6] Peters H. Michael, Cooper W. Douglas, Approximate analytical solutions for particle deposition in viscous stagnation-point flow in the inertial-diffusion regime with external forces, J. Colloid Interface Sci. 142 (1) (1991) 140–148.
[7] R. Tsai, L.J. Liang, Inertial effect on aerosol particle deposition from an axisymmetric stagnation point flow approximation, Int. Commun. Heat Mass Transfer 29 (4) (2002) 489–496.
[8] C.C. Wang, C.K. Chen, Forced convection in micropolar fluid flow over a wavy surface, Numer. Heat Transfer 37 (3) (2000) 271–279.
[9] D.W. Cooper, M.N. Perers, R.J. Miller, Predicted deposition of submicrometer particles due to diffusion and electrostatics in viscous axisymmetric stagnation-point flow, Aerosol Sci. Technol. 11 (2) (1989) 133–143.
[10] P. Wang, R. Kahawita, Numerical integration of partial differential equations using cubic splines, Int. J. Comput. Math. 13 (3–4) (1983) 271–286.